Applied Catalysis B: Environmental 209 (2017) 33–44

Contents lists available at ScienceDirect

Applied Catalysis B: Environmental

journal homepage: www.elsevier.com/locate/apcatb

Activity and stability of Co_3O_4-based catalysts for soot oxidation: The enhanced effect of Bi_2O_3 on activation and transfer of oxygen

Zhou Shang, Min Sun, Sanmao Chang, Xiang Che, Xiaoming Cao, Li Wang*, Yun Guo*, Wangcheng Zhan, Yanglong Guo, Guanzhong Lu

Key Laboratory for Advanced Materials and Research Institute of Industrial Catalysis, School of Chemistry & Molecular Engineering, East China University of Science and Technology, Meilong Road 130, Shanghai, 200237, PR China

ARTICLE INFO

Article history:
Received 30 November 2016
Received in revised form 26 January 2017
Accepted 27 February 2017
Available online 28 February 2017

Keywords:
Soot oxidation
Co_3O_4
Bi_2O_3
Oxygen exchange
Stability

ABSTRACT

Bi_2O_3-Co_3O_4 catalysts were prepared by sol-gel method and tested for soot oxidation by O_2. The composite oxides showed excellent activity under both tight and loose contact when compared with individual Co_3O_4 or Bi_2O_3, and the maximum activity was obtained over catalyst with Bi/Co molar ratio of 0.2. The samples were characterized by means of XRD, N_2 adsorption, FE-SEM, XPS, FT-IR, C-TPR and O_2-TPD. It was found that Bi_2O_3 with low melting point deposited on Co_3O_4 surface could not only promote the contact state between soot and catalyst, but also produce more oxygen species with high mobility and reactivity at Bi-Co interface layer. Oxygen activation channel and reaction pathway were discussed based on the results of isothermal anaerobic titrations and ^{18}O-isotopic tests, which confirmed that soot was more likely to react with lattice oxygen species rather than O_2, especially at low temperatures. The high mobility of lattice oxygen species was attributed to a combination of the O^{2-} conductivity of Bi_2O_3 and the accelerative formation of oxygen vacancies at Bi-Co interface. A feasible reaction mechanism over the binary catalysts for soot oxidation was proposed. The stability tests were also studied and the results indicated that Bi-modified Co_3O_4 showed prominent tolerance against thermal shock, H_2O and SO_2, thus being a promising active component for practical application.

1. Introduction

Soot particulate (mainly carbon nano-particulate), as one of the main hazardous substances in diesel engine exhaust, has seriously adverse impact on environment and public health [1,2]. Diesel particulate filter (DPF) has been proved to be the most reliable and economical after-treatment technology for soot emission control [3–6]. However, the accumulation of soot on the filter's wall will increase the back pressure of DPF and decrease its efficiency, making the timely regeneration of the soot-plugged DPF highly necessary.

As the classical temperatures in diesel engine exhaust pipes (200–400 °C) cannot afford to spontaneous combustion of the deposited soot (above 600 °C) [7], the usage of a high-performance catalyst coated on the wall of DPF (CDPF), which enable to catalyze soot oxidation to CO_2 at relatively low temperatures, is effective to lessen the recline on additional heat sources [8–12].

Co_3O_4 has been proved to behave excellent activity for oxidation reaction due to its strong redox ability [13–18]. For example, Co_3O_4 nanorod with mainly exposed {110} planes could completely convert CO to CO_2 at −77 °C [19]. Moreover, the doping of suitable metal oxide could further promote the activation of oxygen species and accelerate the oxidation reaction on Co_3O_4. Such as, CO could be completely oxidized at as low as −105 °C on In_2O_3-Co_3O_4 catalyst due to the greatly promoted activation of surface oxygen [20]. The interaction between Co_3O_4 and CeO_2 was widely reported to enhance the reactivity of oxygen species which ignited soot under loose contact at much low temperatures [21–24].

For soot catalytic oxidation, known as a typical solid (catalyst) – solid (soot) – gas (O_2) reaction, the contact state between catalyst and soot could obviously influence the reaction rate [25,26]. The doping of metals with lower melting point and higher mobility, such as alkali metals, could "wet" the catalyst surface and promote the contact between catalyst and soot [27–30]. Additionally, the intrinsic activity of the catalyst, especially the reactivity of oxygen species, also plays equally important role [31–34]. Guo et al. demonstrated that the doped K enhanced the activity of lattice oxygen on Co_3O_4 and improved the contact condition between soot

* Corresponding authors.
E-mail addresses: wangli@ecust.edu.cn (L. Wang), yunguo@ecust.edu.cn (Y. Guo).

http://dx.doi.org/10.1016/j.apcatb.2017.02.074
0926-3373/

and catalyst, which jointly contributed to the shift of soot combustion temperatures by ca. 80 °C to lower region [35]. Recently, Obeid et al. reported a fuel-cell type electrochemical mechanism over yttria-stabilized zirconia (YSZ) for soot oxidation based on its bulk oxygen mobility [36], which opens a window for utilizing the materials with superior O^{2-} ions conductivity to promote soot oxidation by accelerating the mobility of reactive oxygen species.

Bi_2O_3 shows high anion conductivity [37] and reducibility [38], which could be used as dopant to improve the redox ability and O^{2-} ions mobility of metal oxides [39,40]. Such as, the presence of bismuth enabled to promote the release and storage of oxygen on CeO_2-ZrO_2 solid solution efficiently at low temperatures attributing to the acceleration of oxide ion migration [41]. The deposition of Bi_2O_3 promoted the activation and mobility of lattice oxygen over Co_3O_4 significantly, which caused the lowest temperature of complete conversion (LTCC) of CO decreasing from −40 °C on pure cobalt oxide to −89 °C on Bi_2O_3-Co_3O_4 [42]. It was also reported that Bi-doped praseodymium oxide exhibited high activity for soot combustion at relatively low temperatures [43]. Therefore, the combination of an oxygen ion conducting material (Bi_2O_3) and a transition metal oxide with great redox capacity (Co_3O_4) might be a powerful strategy to accelerate soot reaction.

In the present work, Bi_2O_3-Co_3O_4 catalysts were prepared by a simple sol-gel method and tested for soot combustion under both tight and loose contact. The effect of Bi_2O_3 on the promoted activity for low-temperature soot oxidation was explored, paying special attention to the role of the catalysts on activation and transfer of oxygen. Meanwhile, the stabilities against thermal shock, water and SO_2, which were also highly desired for a suitable catalyst in practical diesel exhaust purification [44–46], were subsequently examined on the mixed oxides. Moreover, a feasible reaction mechanism was proposed according to the results obtained from this study.

2. Experimental section

2.1. Catalyst preparation

A series of Bi_2O_3-Co_3O_4 catalysts were prepared by the sol-gel method. Metal nitrates with expected stoichiometry were dissolved in dilute nitric acid solution, and mixed with a given amount of citric acid (CA) aqueous solution and polyglycol. The molar ratio of CA to all the metal ions was kept at 1.2:1, and the weight amount of polyglycol was 10% citric acid. The mixed solution was evaporated under stirring at 80 °C until the gel was formed. The resulting gel was dried at 110 °C overnight, followed by the decomposition of nitrates at 450 °C for 2 h and the final calcination at 600 °C for 3 h under static air. The obtained binary catalysts were denoted as Bi_xCo, where x represented the molar ratio of Bi/Co (x = 0.1, 0.2 or 0.3). The referenced pure Co_3O_4 and Bi_2O_3 were obtained by the same method.

2.2. Evaluation of the catalytic performance

Commercial carbon black (CB, Printex-U, Degussa) was used as the model reactant because of its similar reactivity with the real diesel soot [47,48]. The activity of catalyst for soot combustion was evaluated by temperature programmed oxidation experiments (CB-TPO) using a fixed-bed reactor, and an on-line gas chromatograph (GC 9790, Zhejiang Fuli Analytical Instrument Co., China) with an FID detector was used to detect CO_2/CO concentrations in the outlet stream. Typically, a reaction gas of 8% O_2/Ar passed through 50 mg mixture of CB and catalyst (CB/catalyst mass ratio = 1:9) at a flow rate of 100 mL/min. The catalyst and soot were mixed by a spatula briefly to achieve loose contact or by grinding in an agate mortar to get tight contact. 200 mg of inert SiO_2 granules was also added. The reaction temperature elevated from 200 to 650 °C at a heating rate of 5 °C/min after the pretreatment of pure Ar flow at 200 °C for 30 min.

The reaction temperatures corresponding to CB conversions of 10%, 50% and 90% were assigned to T_{10}, T_{50} and T_{90}, respectively.

2.3. Isothermal reaction and anaerobic titration

50 mg tight mixture of catalyst and CB with a mass ratio of 9:1 was used in isothermal reaction. The total flow rate and the reaction gas compositions were the same as those in the TPO reaction. The reaction temperature was fixed at 240 °C to keep the soot conversion below 15%. A series of experiments were conducted to exclude internal and external diffusion according to the method reported elsewhere [49]. When a constant concentration of produced CO_2 was observed, the reaction rate (ν) for soot combustion was calculated.

Isothermal anaerobic titration was subsequently conducted referring to previous researches [49,50]. To avoid the influence of pipeline volume on the response time, the distance between the catalytic bed and the gas chromatograph was as short as possible (ca. 0.5 m). The active oxygen species amount (O^* amount, mol/g) available to soot under these reaction conditions was calculated. TOF value was obtained through dividing reaction rate by O^* amount.

2.4. Isotope oxygen exchange and isotopic soot oxidation reaction

Isotope oxygen exchange or isotopic tracing soot oxidation reaction was performed using $^{18}O_2$, and the products were detected by an online quadrupole mass spectrometer (MS, ICP-400, INFICON). Typically, 100 mg catalyst (isotope oxygen exchange) or catalyst/CB mixture (isotopic tracing soot oxidation reaction) was heated to the desired temperature in a pure He flow of 50 mL/min for 1 h, and then the feed gas was switched to 5000 ppm $^{18}O_2$ in He with a flow of 50 mL/min. The relevant m/e fragments of 28, 30, 44, 46, 48, 32, 34 and 36 were used to monitor $C^{16}O$, $C^{18}O$, $C^{16}O_2$, $C^{16}O^{18}O$, $C^{18}O_2$, $^{16}O_2$, $^{16}O^{18}O$ and $^{18}O_2$, respectively.

2.5. Catalyst characterization

Powder X-ray diffraction (XRD) patterns were recorded on a Bruker D8 diffractometer using Cu Kα radiation and operating at 40 kV and 40 mA. The diffractograms were recorded in 2θ range from 10 to 80° with a step size of 0.02° and a scanning speed of 2°/min. The crystal sizes of Co_3O_4 in different catalysts were calculated by Scherrer formula based on the width of the (311) diffraction peak.

The specific surface areas of the samples were measured using the N_2 adsorption isotherm at −196 °C with BET method through an automatic Micromeritics ASAP 2020 analyzer. The samples were degassed at 200 °C for 2 h prior to the tests.

Inductively coupled-plasma atomic emission spectroscopy (ICP-AES) was conducted on a Varian 710-ES instrument to determine the chemical compositions of the catalysts.

Field emission scanning electron microscopy (FE-SEM) was conducted on a FEI Nova NANOSEM 230 spectrophotometer. The specimens were prepared by pasting of the powder to carbon tape placed on aluminium table.

TG analysis was performed with a PerkinElmer DHG-9146A apparatus. The sample was heated from RT to 800 °C in air flow (100 mL/min).

O_2 temperature programmed desorption (O_2-TPD) was performed in a conventional flow system equipped with a MS detector. The catalysts were pretreated in O_2 flow (20 mL/min) at 500 °C for

30 min, and then cooled down to room temperature (RT) in the same flow. After the removal of gaseous oxygen in pipeline and physical adsorbed oxygen species on the catalyst by He flow at RT, the O_2-TPD was performed from 50 to 700 °C at a heating rate of 10 °C/min in a He flow of 20 mL/min.

Carbon temperature programmed reduction (C-TPR) was performed using the same equipment as that in the TPO reaction. Pure Ar flow passed though the tight mixture of CB and catalyst at a flow rate of 100 mL/min. The reaction temperature elevated from 200 to 650 °C at a rate of 5 °C/min.

Fourier transform infrared (FT-IR) spectra was obtained on a Nicolet Nexus 470 spectrometer. The catalysts were prepared in the form of pressed wafers (ca. 1% sample in KBr). All spectra were generated from a collection of 80 scans at a resolution of 4 cm^{-1}.

X-ray photoelectron spectroscopy (XPS) were performed on a Thermo ESCALAB 250 spectrometer using Al Kα (hν = 1486.6 eV) radiation as the excitation source. Charging of samples was corrected by setting the binding energy of contaminative carbon (C 1s) at 284.8 eV.

2.6. Stability tests

The catalysts were calcinated at 700 or 800 °C for 3 h to investigate the thermal stability, which were expressed as Co_3O_4-700 and Bi_xCo-700 or Co_3O_4-800 and Bi_xCo-800, respectively.

The effects of water on the activities of the catalysts were investigated via the following two aspects: 1) TPO reaction in a steam containing 6% H_2O; 2) hydrothermal pretreatment of the catalyst in the atmosphere containing 6% H_2O + 8% O_2 at 600 °C for 24 h before the normal activity test.

The impact of SO_2 on the catalytic activity was also explored. The catalyst was pretreated at 400 °C in a reaction gas of 1000 ppm SO_2/8% O_2/Ar for 24 h to obtain the sulfated catalyst.

3. Results

3.1. Catalytic performance for soot oxidation

The CB-TPO profiles in 8% O_2/Ar on different catalysts are shown in Fig. 1, and the T_{10}, T_{50} and T_{90} derived from TPO profiles are listed in Table 1. Over the Co-containing catalysts, the selectivity to CO_2 was above 98% due to the high CO oxidation activity of Co_3O_4 [51]. For the oxidation of individual soot, T_{10}, T_{50} and T_{90} were 500, 575 and 625 °C, respectively. The application of catalysts accelerated soot oxidation significantly. Meanwhile, the contact model between catalyst and soot severely affected the activity. Compared with pure Co_3O_4, Bi_2O_3 showed more pronounced activities under both tight- and loose-contact modes.

After the doping of Bi_2O_3, the activity of Co_3O_4 was further improved with introducing bismuth content up to x = 0.2 before decreasing with the further increase of Bi. $Bi_{0.2}Co$ showed the highest activity, and the T_{50} were 332 and 475 °C under tight and loose-contact, respectively, which lowered by 90 and 75 °C compared with those of pure Co_3O_4. As contrasted to $Bi_{0.2}Co$, the mechanical mixture of Co_3O_4 and Bi_2O_3 with the same composition behaved obviously lower active, which implied that the excellent activities of Bi_xCo catalysts were originated from the interaction between Bi_2O_3 and Co_3O_4.

3.2. Structural, textural and morphological characterizations

Fig. 2 illustrates the XRD patterns of Co_3O_4, Bi_xCo and Bi_2O_3. Co_3O_4 showed diffraction peaks corresponding to the spinel-type structure (JCPDS 42-1467). After the introduction of Bi_2O_3, the characteristic peaks of $Bi_2O_2CO_3$ (JCPDS 41-1488) were observed

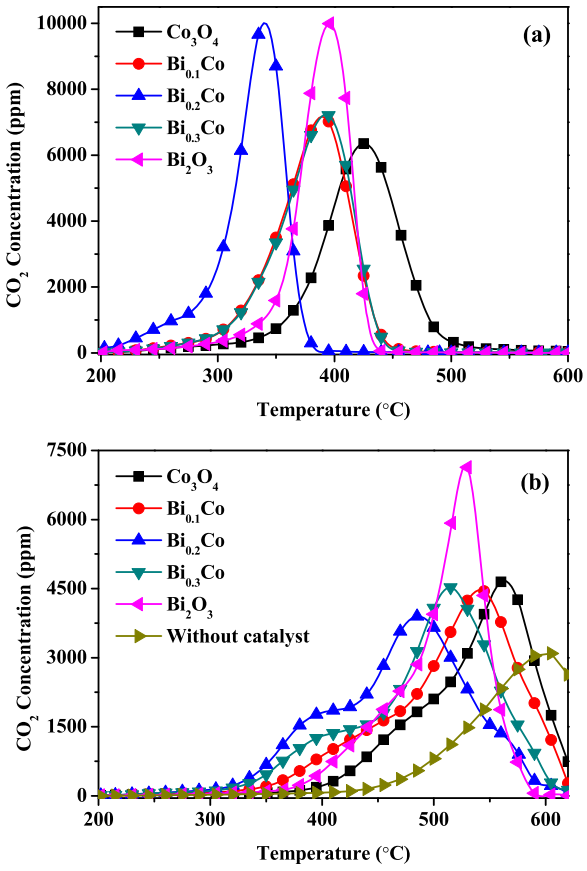

Fig. 1. CB-TPO profiles on Co_3O_4, Bi_2O_3 and Bi_xCo catalysts in 8% O_2/Ar under tight (a) and loose (b) contact.

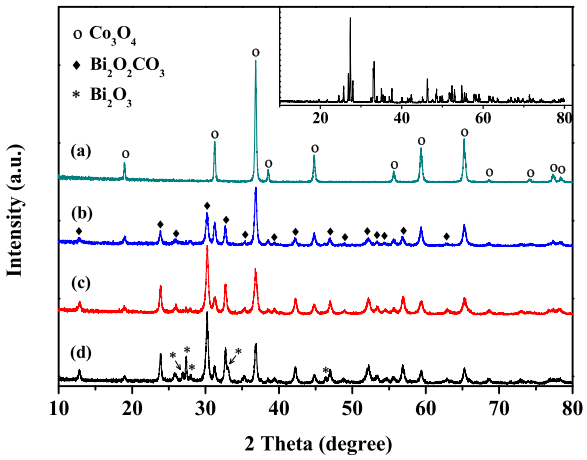

Fig. 2. XRD patterns of Co_3O_4 (a), $Bi_{0.1}Co$ (b), $Bi_{0.2}Co$ (c) and $Bi_{0.3}Co$ (d); the inset is the diffractogram of pure Bi_2O_3.

besides those of cobalt oxide, which was attributed to CO_2 adsorption and storage. However, the result of TG-MS analysis (not shown) demonstrated that the structure of $Bi_2O_2CO_3$ was not stable, it would transform to Bi_2O_3 when the temperature was higher than 200 °C [52]. When Bi content increased to x = 0.3, the diffraction peak of monoclinic Bi_2O_3 (JCPDS 65-2366) could be clearly observed. It should be noted that the as-prepared Bi_2O_3 showed just the monoclinic oxide structure (JCPDS 65-2366, inset in Fig. 2).

In addition, the peaks of Co_3O_4 became broad after the introduction of Bi_2O_3, which indicated that the growth of the crystal Co_3O_4 was suppressed [42]. Indeed, the calculated crystal size based on

Table 1
T_{10}, T_{50} and T_{90} for soot combustion in 8% O_2/Ar over Co_3O_4, Bi_2O_3, Bi_xCo and the mechanical mixture of Co_3O_4 and Bi_2O_3.

Sample	T_{10} (°C)		T_{50} (°C)		T_{90} (°C)		Selectivity (%)	
	Tight	Loose	Tight	Loose	Tight	Loose	Tight	Loose
Co_3O_4	368	460	422	550	466	622	98.6	98.2
$Bi_{0.1}Co$	329	420	381	523	418	582	99.1	98.9
$Bi_{0.2}Co$	281	379	332	475	360	546	99.2	98.8
$Bi_{0.3}Co$	330	394	383	502	419	562	98.7	98.4
Bi_2O_3	350	437	390	513	417	551	96.3	95.6
$Bi_2O_3 + Co_3O_4$[a]	347	436	388	532	420	575	98.3	98.1

[a] The mechanical mixture of Co_3O_4 and Bi_2O_3, Bi/Co molar ratio = 0.2.

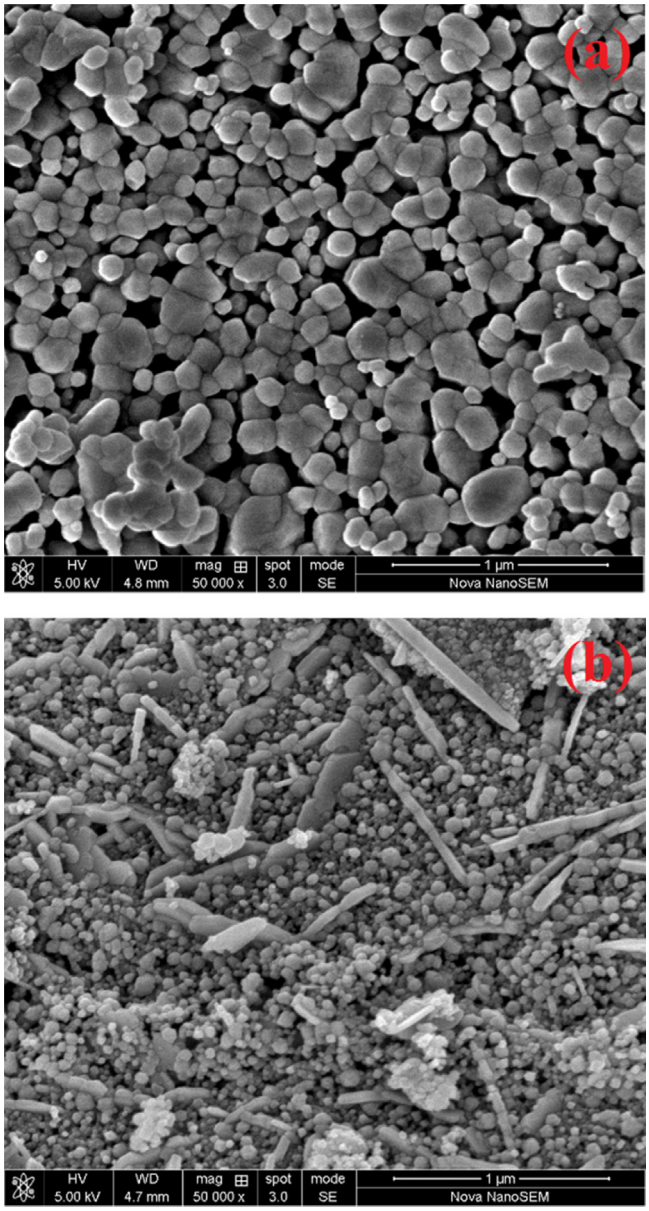

Fig. 3. FE-SEM images of Co_3O_4 (a), $Bi_{0.2}Co$ (b).

Scherrer equation was 37.3 nm for Co_3O_4, while these were 26.6, 21.5 and 25.8 nm for $Bi_{0.1}Co$, $Bi_{0.2}Co$ and $Bi_{0.3}Co$, respectively.

Fig. 3 shows the FE-SEM images of Co_3O_4 and $Bi_{0.2}Co$ samples. Co_3O_4 was consisted of the aggregations of irregular particulates with sizes varying from ca. 35–250 nm (Fig. 3a). While after the deposition of Bi_2O_3 (Fig. 3b), the catalyst surface became more rough and the sizes of the irregular particulates decreased to ca. 10–100 nm, in accordance with the crystal size results from XRD.

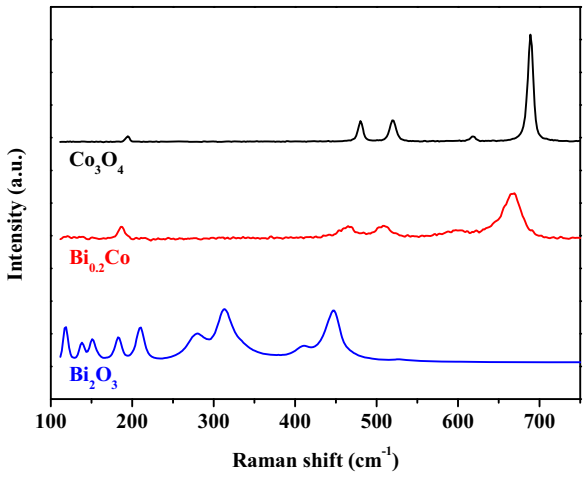

Fig. 4. Raman spectra of Co_3O_4, $Bi_{0.2}Co$ and Bi_2O_3.

The BET surface areas of the catalysts are listed in Table 2. All the samples showed similar BET surface areas in the range of 10.4–15.3 m^2/g except for Bi_2O_3, which had the lowest value of 1.8 m^2/g. Combined with the results in Fig. 1 and Table 1, the conclusion could be drawn that the BET surface area of catalyst was not a key to decide the activity for soot combustion.

Raman spectra of Co_3O_4, Bi_2O_3 and $Bi_{0.2}Co$ are shown in Fig. 4. For pure Bi_2O_3, the Raman peaks from 100 to 500 cm^{-1} were the characteristic peaks of the monoclinic α-Bi_2O_3 [53]. While for pure Co_3O_4, there were five Raman-activated modes: the bands at 688, 618, 520, 480 and 194 cm^{-1} were assigned to the A_{1g}, $F_{2g}^{(3)}$, $F_{2g}^{(2)}$, E_g and $F_{2g}^{(1)}$ symmetry of crystalline Co_3O_4 [20]. On $Bi_{0.2}Co$ sample, no Raman peaks corresponding to bismuth oxide appeared, and the Raman peaks of crystalline Co_3O_4 shifted to lower frequencies and became broad, which originated from the change of the original coordinative environment of cobalt sites in spinel structure, indicating that the doping of Bi_2O_3 caused the lattice distortion or residual stress. This phenomenon had already been demonstrated to be a sign for the weakening of the Co—O bond strength and the formation of oxygen vacancy on Co_3O_4 [20,54].

3.3. C-TPR

C-TPR was used to investigate the availability and mobility of lattice oxygen species for soot oxidation, and the C-TPR profiles of the as-prepared catalysts are exhibited in Fig. 5. Co_3O_4 showed a broad reduction peak in the temperature range of 475–600 °C with maximum at 530 °C. Bi_2O_3 behaved similarly in the reduction process with reduction peak slightly shifting by ca. 15 °C to lower temperatures.

Table 2
Surface area and calculated values obtained from isothermal anaerobic titrations at 240 °C.

Sample	Surface area (m^2/g)	Rate ($mol\ s^{-1}\ g^{-1} \times 10^{-7}$)	Specific rate ($mol\ s^{-1}\ m^{-2} \times 10^{-8}$)	O* amount ($mol\ g^{-1} \times 10^{-4}$)	TOF ($s^{-1} \times 10^{-3}$)
Co_3O_4	12.1	1.03	0.86	0.63	1.64
$Bi_{0.1}Co$	12.0	4.80	3.98	2.77	1.73
$Bi_{0.2}Co$	15.3	8.07	5.26	4.55	1.78
$Bi_{0.3}Co$	10.4	1.64	1.58	0.94	1.74
Bi_2O_3	1.8	0.56	3.03	0.41	1.37

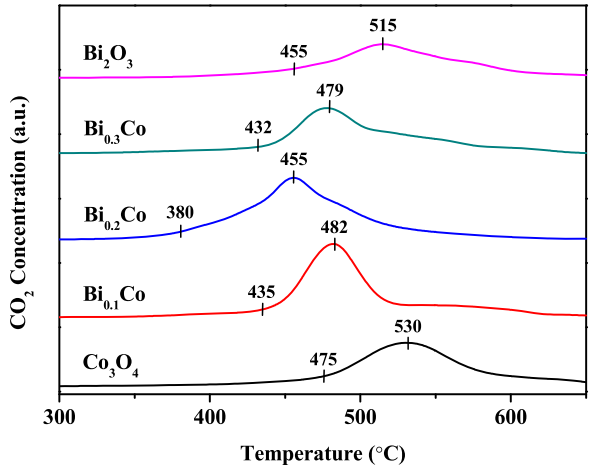

Fig. 5. C-TPR profiles of Co_3O_4, Bi_xCo and Bi_2O_3 samples.

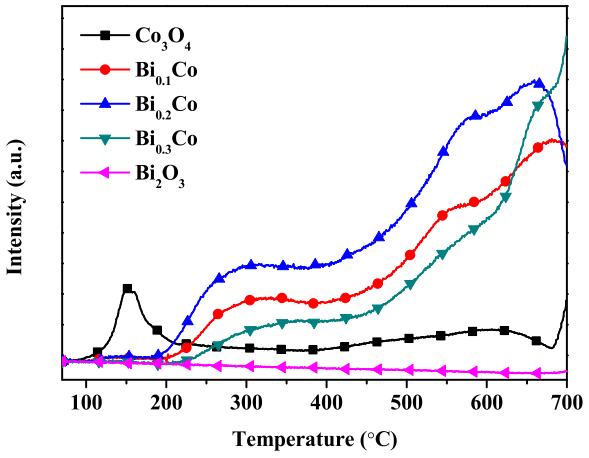

Fig. 6. O_2-TPD profiles of Co_3O_4, Bi_2O_3 and Bi_xCo samples.

After the deposition of Bi_2O_3, the reduction peaks of Bi_xCo shifted to lower temperatures with the increase of Bi_2O_3 content in the form of a volcano trend. Among them, $Bi_{0.2}Co$ exhibited the lowest onset and peak temperatures at 380 and 455 °C, respectively. It is well known that the lower the reduction temperature for C-TPR, the more facile activation of lattice oxygen. Compared with pure Co_3O_4, the shift of reduction curves to lower temperatures by ca. 40–95 °C showed that the activation of lattice oxygen on Bi_xCo was promoted significantly. Moreover, after C-TPR test, the decrement of the initial soot on $Bi_{0.2}Co$ was the largest, achieving 48%, which was much higher than that on Co_3O_4 (35%) and Bi_2O_3 (28%), which implied that the mobility of lattice oxygen was enhanced and the amount of active oxygen species was increased by modifying Co_3O_4 with Bi_2O_3.

Compared with the results in Fig. 1, a defined correlation between the peak temperatures of TPO and C-TPR was obtained on Bi_xCo catalysts, which indicated that the activation and mobility of lattice oxygen promoted by the interaction between Co_3O_4 and Bi_2O_3 played crucial roles on soot oxidation.

3.4. O_2-TPD

As mentioned above, the activation and mobility of oxygen species on the surface and in the bulk of a catalyst has an important contribution to soot oxidation activity [23]. And thus, O_2-TPD experiments were conducted to further confirm the promoted effect of Bi_2O_3 on the activation of oxygen species for Co_3O_4-based catalysts, and the results are shown in Fig. 6.

Bi_2O_3 showed no desorption of oxygen in the temperature range of 100–700 °C. Remarkable releases of O_2 were observed above 700 °C for all Co-containing samples, which was attributed to the thermal decomposition of Co_3O_4 to CoO [55]. For Co_3O_4, a peak was observed at ca. 150 °C corresponding to the weakly adsorbed oxygen [56]. Combined with the results in Table 1, the onset temperature (T_{10}) of soot oxidation over Co_3O_4 was much higher than it, which demonstrated that this oxygen species might be not involved in soot oxidation reaction [57].

When focusing on the temperatures above 200 °C, corresponding to the temperature range of soot ignition, noticeable release of oxygen was observed over Bi_xCo catalysts certainly originating from the interaction between Co_3O_4 and Bi_2O_3, and the desorption amount increased with the Bi content in a volcano-type form. $Bi_{0.2}Co$, with the highest activity for soot oxidation, desorbed the maximum quantity of oxygen in the range of 200–700 °C.

It was suggested that over Bi_xCo, the strong synergetic effect between Co_3O_4 and Bi_2O_3 could weaken the strength of metal—O bond, improve the release ability of lattice oxygen and decrease the formation energy of oxygen vacancies, a descriptor of oxidation reactivity for metal oxide [58], at Bi-Co interface. Meanwhile, the presence of Bi_2O_3 could accelerate the oxygen diffusion from bulk to complement the produced oxygen vacancy at the interface due to its high oxygen ion conductivity [37], which further promoted the desorption of O_2. Therefore, the significant desorption behavior of O_2 on Bi_xCo demonstrated that the amount and mobility of oxygen species were obviously enhanced, which could be involved in soot oxidation at the contact points between catalyst and soot.

3.5. XPS

XPS characterization was performed to investigate the surface chemical state of the catalysts, and the O 1s spectra are shown in Fig. 7. As seen, broad O 1s spectra were observed for both Co_3O_4 and $Bi_{0.2}Co$. Peak deconvolution and fitting was conducted, and the results revealed that both samples are comprised of three well-defined components, namely O_α, O_β and O_γ species at binding energy of ca. 529.6–530.0 eV, 530.2–530.8 eV and 531.3–531.7 eV, respectively, corresponding to surface lattice oxygen, surface adsorbed oxygen and the oxygen in the water and carbonate [49,59]. Subsequently, the ratios of $O_\alpha/(O_\alpha + O_\beta + O_\gamma)$ obtained were 32% and 56% over Co_3O_4 and $Bi_{0.2}Co$, respectively, which indicated the exposure of more lattice oxygen species on $Bi_{0.2}Co$ surface.

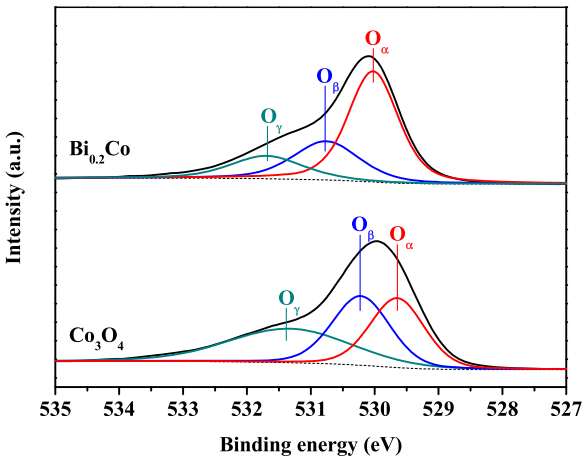

Fig. 7. O 1s XPS of Co_3O_4 and $Bi_{0.2}Co$ samples.

It is well accepted that the charge on the oxide ions was significantly influenced by their surrounding chemical environment, and the nature of the dopant ions would decide the shifts of O 1s binding energy to either side [60]. A slight shift of binding energy (ca. 0.4 eV) for O 1s was found over $Bi_{0.2}Co$ compared with that of Co_3O_4, which implied the formation of Co—O—Bi type bond at the interface layer due to the strong interaction between these two oxides in Bi_xCo samples.

3.6. Isotopic exchange reaction of oxygen

To further explain the activation mechanism of gaseous oxygen on Bi_xCo catalysts, isotopic $^{18}O_2$ exchange reactions over Co_3O_4 and $Bi_{0.2}Co$ were conducted and the results are shown in Fig. 8. After the introduction of $^{18}O_2$ over Co_3O_4 at 300 °C (Fig. 8a), the signal $^{18}O_2$ (36) was observed immediately and reached equilibrium after ca. 500 s. The signals of $^{16}O_2$ (32) and $^{16}O^{18}O$ (34) evolved almost synchronously, which got their maximums after 100–130 s and then decreased gradually with time. When increasing the reaction temperature to 400 °C (Fig. 8b), $^{18}O_2$ was detected at ca. 20 s after it being introduced into the reactor, which indicated that the exchange reaction between $^{18}O_2$ and surface oxygen on catalyst became more drastic with the increasing of reaction temperature. Meanwhile, $^{16}O^{18}O$ signal became more apparent with respect to $^{16}O_2$, which demonstrated that the oxygen exchange between one atom of gaseous O_2 and one atom of catalyst oxygen was promoted at the higher temperatures. Continuously increasing the temperature to 500 °C, the exchange behavior of $^{18}O_2$ was similar to that of 400 °C, with the retention time of $^{18}O_2$ signal being further extended to ca. 30 s.

The presence of Bi_2O_3 changed the behavior of $^{18}O_2$ exchange on Co_3O_4 obviously. At 300 °C (Fig. 8d), once $^{18}O_2$ was introduced, the signal of $^{16}O_2$ observably risen to the peak value, which was comparable with the inlet $^{18}O_2$ concentration, and then decayed gradually. The appearance of $^{18}O_2$ was slightly lagged behind that of $^{16}O_2$. In the meantime, $^{16}O^{18}O$ could not be detected at the beginning 30 s, then its signal intensity increased gradually and reached equilibrium after ca. 800 s. For the exchange reaction at 400 °C (Fig. 8e), the apparent differences were found in the intensity changes of $^{18}O_2$ and $^{16}O^{18}O$ with the reaction time. The intensity of $^{16}O^{18}O$ signal increased significantly and got the peak value after ca. 750 s. Furthermore, $^{18}O_2$ was detected at ca. 50 s after the introduce of $^{18}O_2$ in the feed gas, and its intensity increased slowly with the increasing of reaction time, and reached the equilibrium after ca. 3800 s. At 500 °C (Fig. 8f), $^{18}O_2$ was detected at ca. 550 s, which further lagged behind that of 300 and 400 °C, indicating that more lattice oxygen species were activated and exchanged.

The oxygen exchange reactions were undoubtedly more drastic over $Bi_{0.2}Co$ than that on Co_3O_4. Estimated ^{18}O-atoms exchange amount ratios of $Bi_{0.2}Co/Co_3O_4$ were ca. 1.5, 6.6 and 12.1 at 300, 400 and 500 °C, respectively, indicating that more oxygen species with high mobility was involved in the exchange on $Bi_{0.2}Co$. Meanwhile, the evolution of $^{16}O_2$ on $Bi_{0.2}Co$ was always steeper than that of $^{16}O^{18}O$ at initial stage of exchange reaction under the tested temperatures, which was different from the results on Co_3O_4.

In general, there are two possible mechanisms for gaseous $^{18}O_2$ to exchange its atoms with the oxide, namely R^1- and R^2-mechanism [61]:

The first is the exchange between an atom from oxygen molecule and an atom from the oxide (R^1-mechanism, simple heteroexchange):

$$^{18}O_2(g) + {}^{16}O(s) \rightarrow {}^{18}O^{16}O(g) + {}^{18}O(s)$$

The second is that the oxygen molecule exchanges both atoms with two atoms from the oxide (R^2-mechanism, multiple heteroexchange).

$$^{18}O_2(g) + 2{}^{16}O(s) \rightarrow {}^{16}O_2(g) + 2{}^{18}O(s)$$

It was likely that for Co_3O_4, R^1-mechanism was more dominant, especially at higher temperatures (above 400 °C), because the formation of $^{16}O^{18}O$ was more prevalent, which meant that the dissociative adsorption of gas oxygen and the following oxygen exchange with catalyst surface oxygen were more rapid than oxygen transfer from surface to the bulk [62,63]. However, the isotopic exchange on $Bi_{0.2}Co$ showed $^{16}O_2$ was the primary exchange product, and $^{16}O^{18}O$ was produced only when the $^{16}O_2$ got its maximum, which was the characteristic of R^2-mechanism and implied that bulk-surface diffusion was sufficiently fast for bulk oxygen to participate in oxygen exchange [63]. In other words, the proportion of R^2-mechanism was enhanced by doping Co_3O_4 with Bi_2O_3. For R^1-mechanism O_2 exchange occurs at one vacant surface site, while for R^2-mechanism two adjacent vacant surface sites are required to decompose the adsorbed gas-phase oxygen [61,64–66]. Therefore, it was reasonable that doped Bi_2O_3 facilitated the formation of plenty oxygen vacancies and rapid delivery of lattice oxygen between Bi-Co interface and Bi_2O_3.

3.7. Isothermal reaction and kinetic parameters

Isothermal reaction and anaerobic titration at 240 °C were conducted to gain more insights into the reaction mechanism over Co_3O_4, Bi_2O_3 and Bi_xCo catalysts. The quantified values of the reaction rate, active oxygen amount (O* amount) and TOF are summarized in Table 2.

As can be seen, TOF value sequence was $Bi_{0.2}Co > Bi_{0.1}Co \approx Bi_{0.3}Co > Co_3O_4 > Bi_2O_3$, and the soot oxidation rate of Bi_xCo increased significantly with increasing Bi_2O_3 content up to x = 0.2. The $Bi_{0.2}Co$ showed the much higher specific rate value (5.26×10^{-8} mol s^{-1} m^{-2}) than that of Co_3O_4 (0.86×10^{-8} mol s^{-1} m^{-2}) or Bi_2O_3 (3.03×10^{-8} mol s^{-1} m^{-2}) in spite of its largest surface area, which demonstrated that doping Co_3O_4 with Bi_2O_3 produced more active reaction sites for soot oxidation due to the strong interaction between them.

The values of O* amount on the catalysts revealed that the introduction of Bi_2O_3 obviously increased the number of active oxygen species from 0.63×10^{-4} mol/g on Co_3O_4 to $0.94 - 4.55 \times 10^{-4}$ mol/g on Bi_xCo. Moreover, O* amounts on $Bi_{0.1}Co$ and $Bi_{0.2}Co$ were an order of magnitude higher than those of other catalyst systems like Fe-CeO_2 ($3.45 - 5.72 \times 10^{-5}$ mol/g) and three-dimensionally ordered macroporous $La_{1-x}K_xCoO_3$

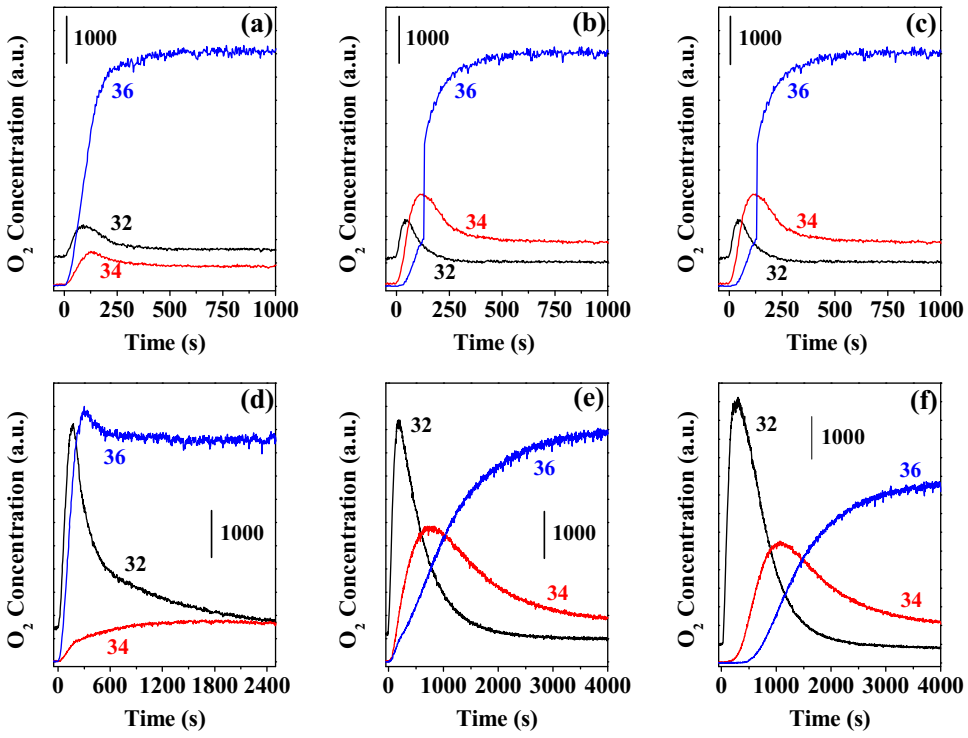

Fig. 8. $^{18}O_2$-exchange reaction profiles over Co_3O_4 (a–c) and $Bi_{0.2}Co$ (d–f) in 5000 ppm $^{18}O_2$/He. The reactions were conducted at 300 (a and d), 400 (b and e) and 500 °C (c and f), respectively.

($4.14 - 4.99 \times 10^{-5}$ mol/g) reported elsewhere [49,50]. This results showed that more oxygen species was involved in the soot oxidation on Bi_xCo catalysts, which was believed to be related to their excellent ability to deliver lattice oxygen to soot particulate.

3.8. Isothermal oxidation of soot over $Bi_{0.2}Co$ by $^{18}O_2$

To further investigate the soot reaction process over $Bi_{0.2}Co$ catalysts, isothermal oxidation of soot by $^{18}O_2$ was conducted and the results are shown in Fig. 9. In order to better identify the ability of catalyst for the oxygen diffusion, 5000 ppm $^{18}O_2$ in He was used in the reaction.

For the reaction at 200 °C under tight contact mode (Fig. 9a), reaction rate was quite slow due to the low reaction temperature. The gaseous products of soot oxidation were almost the $C^{16}O_2$, and the species containing ^{18}O were barely observed. Meanwhile, the decrease of CO_2 concentration after the initial 500 s might be attributed to the depletion of the most active C free sites on soot surface [67].

Elevating the reaction temperature to 300 °C (Fig. 9b), soot oxidation rate was accelerated greatly, and the amount of CO_2 (including $C^{16}O_2$, $C^{16}O^{18}O$ and $C^{18}O_2$) produced was obviously increased. Furthermore, the rapid increases of $C^{16}O_2$ and $C^{16}O^{18}O$ concentrations were observed after the introduction of $^{18}O_2$ in feed gas, with that of $C^{16}O_2$ more prominently. The formation rate of $C^{18}O_2$ was much lower than that of $C^{16}O_2$ and $C^{16}O^{18}O$, whose signal intensity increased gradually with the increasing of reaction time. $C^{18}O_2$ became the dominant product only after ca. 1000s. Compared the inset in Fig. 9b with the result in Fig. 8d, the peak of $^{16}O_2$ in the beginning stage of the exchange reaction disappeared in the process of soot oxidation, which indicated that the highly mobile lattice oxygen species were very active and easily reacted with soot at relatively low temperatures.

For the reaction under loose contact at 400 (Fig. 9c) and 500 °C (Fig. 9d), similar results were obtained. The sequence of the formation rate of three products at the initial phase of reaction was the same as that under tight contact, i.e. $C^{16}O_2 > C^{16}O^{18}O > C^{18}O_2$. Different ^{18}O content proportions in product were found between reactions at 400 (Fig. 9c) and 500 °C (Fig. 9d), and the ^{18}O content in CO_2 at 400 °C was lower than that at 500 °C, which implied that more lattice oxygen species was involved at lower temperatures than gaseous oxygen. Additionally, the peaks of signal $^{16}O_2$ (32) and $^{16}O^{18}O$ (34) in oxygen exchange reaction (Fig. 8e and f) likewise weakened or vanished during soot reaction under loose contact, which further confirmed a correlation between oxygen exchange ability of the catalyst and its catalytic activity for soot oxidation: at appropriate temperature range, the larger the quantity of oxygen in oxide involved in exchange reaction, the higher catalytic activity for soot combustion [36,68,69].

3.9. Impact of SO_2 treatment on Co_3O_4 and $Bi_{0.2}Co$ catalyst

The FT-IR spectra of fresh and SO_2-treated samples in wavenumber range of 900–2000 cm^{-1} are shown in Fig. 10. All samples presented band at 1630 cm^{-1} which was related with the bending OH vibrations of physisorbed water [70]. The small band presented on $Bi_{0.2}Co$ at 1389 cm^{-1} was assigned to antisymmetric N—O stretching band typical of free nitrate ions [71], which was due to incomplete decomposition of the nitrate precursors.

As can be seen, after the pretreatment in 1000 ppm SO_2 for 24 h, a broad band from 980 to 1380 cm^{-1} and centralized at 1114 cm^{-1} appeared on both Co_3O_4 and $Bi_{0.2}Co$, which was related to the S=O functionality [72], indicating the formation of sulfates. However, the intensity of this band was obviously less on $Bi_{0.2}Co$ than that on Co_3O_4.

Table 3 summarizes the results of XPS and activity obtained before and after sulfation. The S surface content of Co_3O_4 (11.0%) was more than that of $Bi_{0.2}Co$ (2.0%) after SO_2 treatment, which indicated that the presence of Bi_2O_3 suppressed the deposition of sulfates on the catalyst surface, coinciding with the FT-IR results

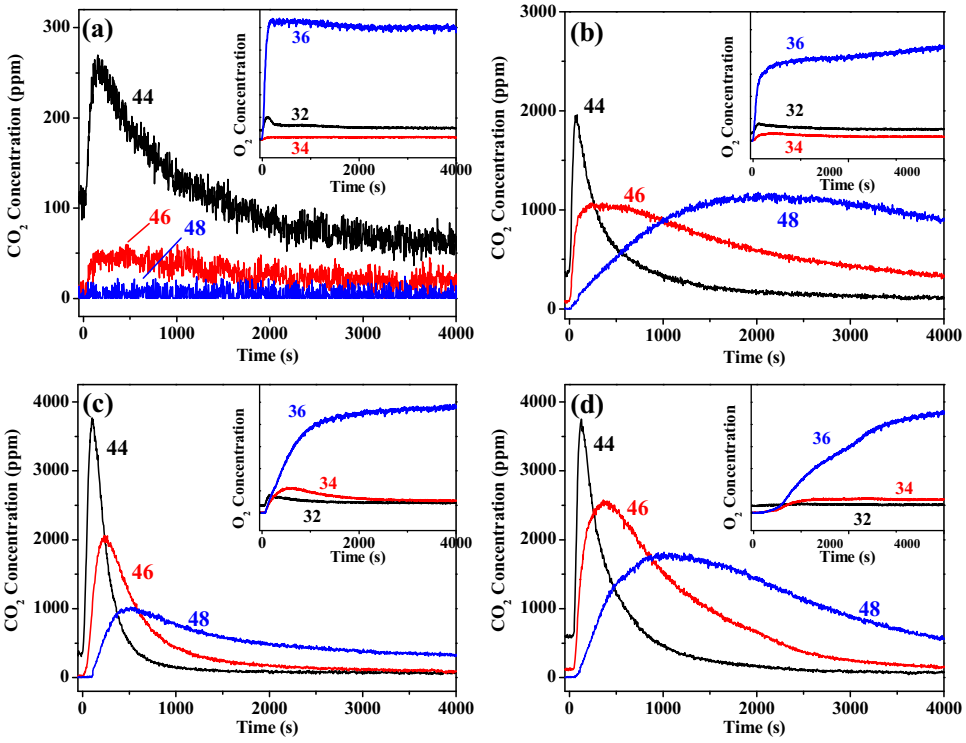

Fig. 9. Isothermal oxidation of soot over $Bi_{0.2}Co$ in 5000 ppm $^{18}O_2$/He. The reactions are conducted under tight contact at 200 (a) and 300 °C (b), or under loose contact at 400 (c) and 500 °C (d). Inset is the evolution curve of the gaseous oxygen species ($^{16}O_2$, $^{16}O^{18}O$ and $^{18}O_2$) during the soot oxidation reaction.

Table 3
Surface composition and activity of fresh and SO_2-treated Co_3O_4 and $Bi_{0.2}Co$ catalysts.

Sample	Surface composition (%)[a]				Loose contact mode	
	Co	Bi	O	S	T_{50} (°C)	Selectivity (%)
Co_3O_4	36.6	\	63.4	\	550	98.8
Co_3O_4, 24 h SO_2 treated	19.1	\	69.9	11.0	565	69.7
$Bi_{0.2}Co$	25.8	12.3	61.9	\	475	99.2
$Bi_{0.2}Co$, 24 h SO_2 treated	30.5	8.0	59.5	2.0	460	98.1

[a] Obtained from XPS analysis: The surface composition was corrected by deducting the carbon content and subsequent normalization; The \ entry stands for N.A. (Not Available).

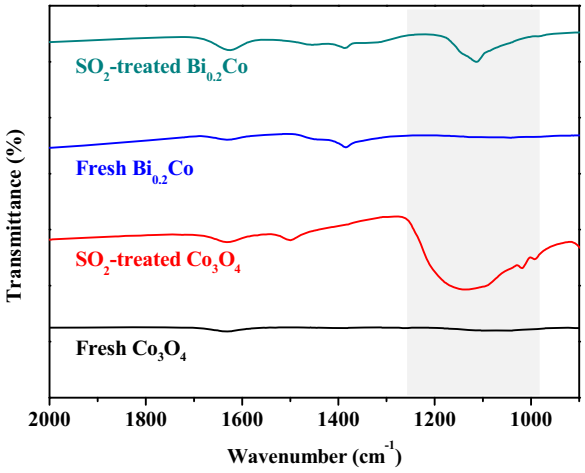

Fig. 10. FT-IR spectra of fresh and SO_2-treated samples.

in Fig. 10. Additionally, the Co surface content of Co_3O_4 distinctly decreased from 36.6% on the fresh one to 19.1% on the sulfated one. While the change was reverse on $Bi_{0.2}Co$ showing a slight increase of surface Co content from 25.8% to 30.5% after sulfation.

For the impact of SO_2 on soot oxidation activity, there were still some debatable conclusions in the open literatures. SO_2 either promoted or poisoned the catalysts depending upon the compositions of the catalytic formulations and the reaction conditions [73–76]. However, for the most cases, SO_2 could be oxidized to produce SO_3 and subsequently deposited on catalyst surface in the form of stable sulfate species, which would result in the severe deactivation of Co_3O_4 after being exposed to SO_2 [77].

In the present work, as expected, the activity of pure Co_3O_4 decreased after exposed to SO_2 for 24 h. Especially, the selectivity of CO_2 showed an obvious decline from 98.1% to 69.7%, which suggested that the deposited sulfates on Co_3O_4 surface severely inhibited its oxidation ability for CO. However, the activity of $Bi_{0.2}Co$ was promoted and the T_{50} of soot oxidation shifted to lower temperature after pretreating in SO_2 for 24 h, and the selectivity of CO_2 still remained stable. It was explained by the fact that the presence of Bi_2O_3 on catalyst surface might produce some acid sites which could suppress the deposition of SO_3 to some extent

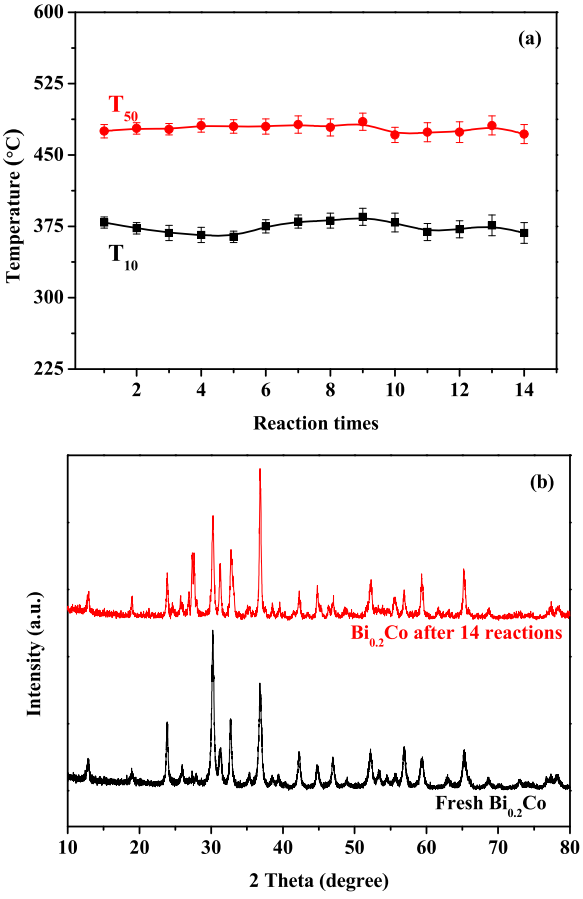

Fig. 11. (a) T_{10} and T_{50} for soot oxidation under loose contact over $Bi_{0.2}Co$ catalyst in 14 times of TPO recycles; (b) XRD patterns of the fresh and reacted $Bi_{0.2}Co$.

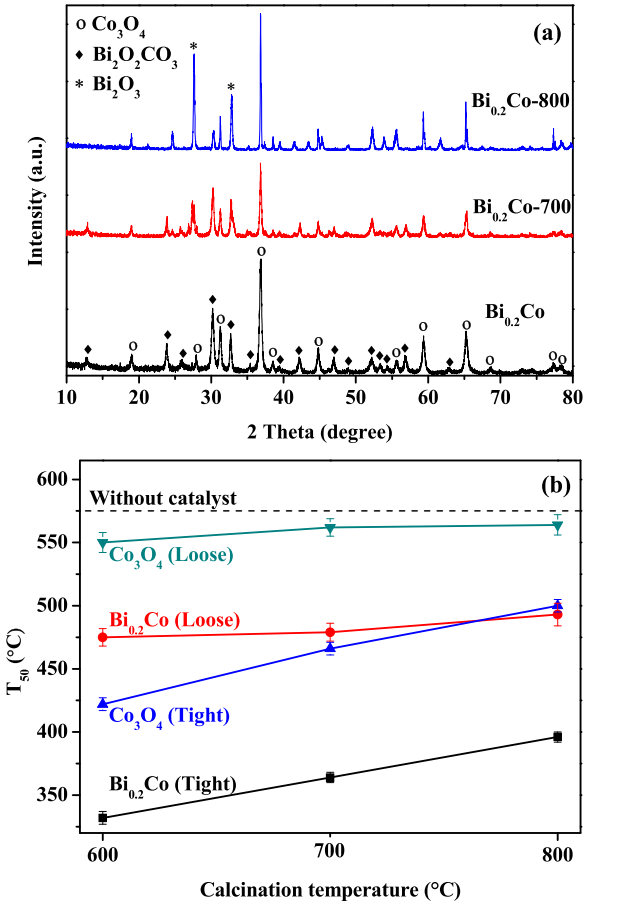

Fig. 12. (a) XRD patterns of $Bi_{0.2}Co$, $Bi_{0.2}Co$-700 and $Bi_{0.2}Co$-800; (b) T_{50} under tight or loose contact over Co_3O_4 and $Bi_{0.2}Co$ catalysts calcined at different temperatures.

[78,79]. Meanwhile, after SO_2 exposure, a moderately enhanced surface acidity could further promote soot oxidation by accelerating the decomposition of the reactive intermediate species [80].

3.10. Recycle and thermal stability of $Bi_{0.2}Co$ catalyst

The recycle stability test of $Bi_{0.2}Co$ was conducted and the loose contact mode was adopted in consideration that this contact mode was more closed to the real situation between catalysts and soot in CDPF [81]. After one activity evaluation, the catalyst powder was taken out from the reactor and mixed with soot carefully to avoid the mass loss, and this loss had been successfully kept below 10% after 14 tests.

As can be seen in Fig. 11a, the activity of $Bi_{0.2}Co$ could be maintained during the 14 times TPO recycles, and only a minor oscillation (less than 15 °C) was found both on the T_{10} and T_{50} evolution curves. XRD results (Fig. 11b) showed that after 14 reactions, the relative intensities of the $Bi_2O_2CO_3$ diffraction peaks decreased because of the decomposition of this species to Bi_2O_3 during the reaction. Meanwhile, the BET surface area of $Bi_{0.2}Co$ after 14 reactions, 15.1 m^2/g, was very similar to the fresh one (15.3 m^2/g). These results indicated that $Bi_{0.2}Co$ behaved high operational stability and reproducibility.

Fig. 12a shows the XRD patterns of $Bi_{0.2}Co$ calcined at different temperatures, and the assignment of the diffraction peaks was consistent with those in Fig. 2. The calculated crystal sizes of Co_3O_4 based on (311) diffraction peak were 21.5, 30.8 and 60.4 nm for $Bi_{0.2}Co$, $Bi_{0.2}Co$-700 and $Bi_{0.2}Co$-800, respectively, which showed that high temperature (ca. 800 °C) caused the sintering of the catalysts. Additionally, the BET surface area decreased from 15.34 m^2/g for $Bi_{0.2}Co$ to 7.06 m^2/g for $Bi_{0.2}Co$-800.

Fig. 12b shows the impacts of calcination temperatures on the activities of Co_3O_4 and $Bi_{0.2}Co$ catalysts for soot oxidation. Under tight contact, T_{50} increased linearly with the calcination temperatures. Moreover, as the increase of the calcination temperature from 600 to 800 °C, the deactivation was more severe over Co_3O_4 which showed an increase of T_{50} by ca. 90 °C, while that was only 65 °C over $Bi_{0.2}Co$. Under loose contact, the change of T_{50} seemed less obvious over Co_3O_4 (ca. 15 °C). However, compared with the situation without catalyst, T_{50} of Co_3O_4-800 showed an only 10 °C lowering, which indicated that the promoted role of Co_3O_4-800 was slight. While for $Bi_{0.2}Co$ and $Bi_{0.2}Co$-700, they had the similar activities, and only an increment of 35 °C was found when increased the calcination temperature to 800 °C. Hence, the modification of Bi_2O_3 enhanced the thermal stability of Co_3O_4 catalysts for soot oxidation, especially under loose contact.

3.11. Impact of water on $Bi_{0.2}Co$ catalyst

The T_{50} over $Bi_{0.2}Co$ in steam containing 6% H_2O and normal feed gas are shown in Fig. 13. The presence of H_2O in feed gas was beneficial to lower the temperatures of soot combustion, especially for the loose contact mode, under which the T_{50} lowered by ca. 45 °C in the presence of 6% H_2O. This promoted effect of H_2O might be ascribed to the wetting role, just like that of K, which improved the contact between catalyst and soot [82]. Meanwhile, the presence of H_2O could also stimulate the hydrolysis of the intermediates formed

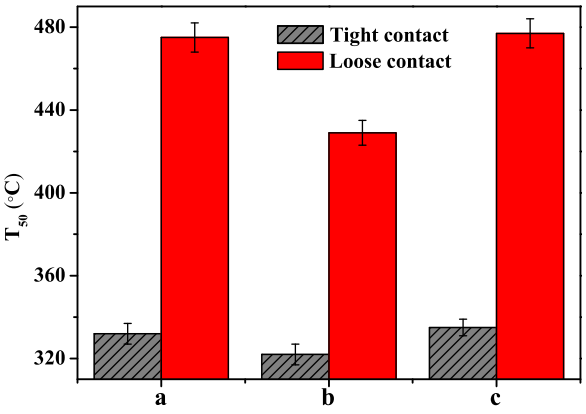

Fig. 13. T_{50} over $Bi_{0.2}Co$ catalyst under tight and loose contact in normal feed gas (a and c) and in steam containing 6% H_2O (b): (a) fresh catalyst; (c) the catalyst after hydrothermal aging pretreatment in 6% H_2O + 8% O_2/Ar at 600 °C for 24 h.

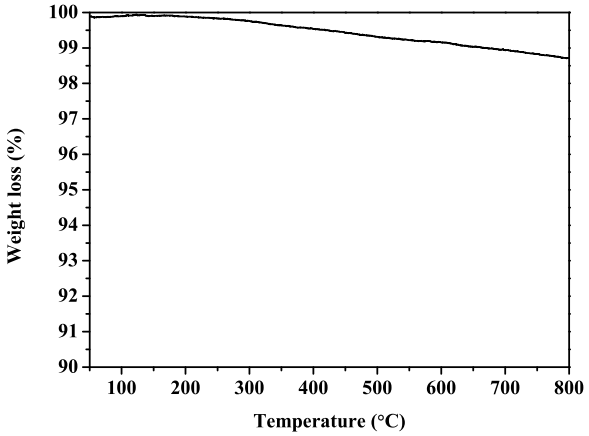

Fig. 14. TG analysis of Bi_2O_3 sample.

during the soot oxidation process [74], which also facilitated the soot oxidation reaction.

Besides, hydrothermal (HT) aging was also conducted and the results in Fig. 13c showed that the activity of $Bi_{0.2}Co$ almost unchanged even after HT aging at 600 °C for 24 h, which indicated that $Bi_{0.2}Co$ catalyst behaved high hydrothermal stability.

4. Discussion

For soot oxidation reaction, the catalysts with low melting points were widely reported because of their promotion for the contact state between catalyst and soot [83,84]. Such as, Serra et al. found that during the soot oxidation over Cu-K-V catalysts, eutectic liquid phases were formed at the temperature closed to soot ignition, which could 'wet' the catalyst surface and contribute to the enhanced activities of the catalysts [85]. Zachariah et al. also studied the reaction between carbon and Bi_2O_3, CuO or Fe_2O_3 by SET/TEM and EDS [86,87]. They found morphological changes of metal oxides before and after reaction and suggested the mobility of melting metal oxide species. Indeed, the melting point of Bi_2O_3 was relatively low [88], which made Bi_2O_3 behave higher activity for soot oxidation than Co_3O_4 (Fig. 1 and Table 1). And in Bi_xCo catalysts, some Bi species away from Co_3O_4 surface, namely not strongly interacting with Co_3O_4, might have high mobility at temperatures closed to the Tammann temperature and result in more junctions of carbon and catalyst, and further the promotion of catalytic activities.

On the other hand, some molten salts might be easy to evaporate causing the severe deactivation of the catalyst and the emission of metal salt into the environment, so we conducted the TG analysis of pure Bi_2O_3 to reveal the possible loss of Bi species. As shown in Fig. 14, when the temperature increased from 100 to 800 °C, only a weight loss of ca. 1.2% was observed, which included the release of H_2O coming from the surface hydroxyl and CO_2 coming from the decomposition of the surface residual carbonaceous species. Meanwhile, even though after 14 times reactions, $Bi_{0.2}Co$ catalyst showed similar activity compared with the fresh catalyst (Fig. 11), and the ICP-AES analysis demonstrated that the Bi/Co molar ratio slightly decreased from 0.197 on the fresh one to 0.195 on the 14-times reacted one. All those results indicated that bismuth species was relatively stable even at temperatures as high as 800 °C.

More importantly, although Bi_2O_3 could improve the contact state between catalyst and soot, T_{50} of soot oxidation on Bi_xCo were still much lower than that on the mixture of Co_3O_4 and Bi_2O_3. Hence, the synergetic interaction between Co_3O_4 and Bi_2O_3 was suggested to be the more important factor influencing the catalytic activity of Bi_xCo catalysts for soot oxidation.

For composite catalysts, the interaction between different components might enhance the ability for oxygen activation by mutual interference of chemical bonding [89–93]. For example, the metal-metal oxide interface could stimulate the mobility of lattice oxygen [94] or adsorbed oxygen species [95,96]. Bueno-López et al. [97] showed that the activities of copper catalysts for soot oxidation were influenced positively by the supports because the interaction between Cu and the support could improve the redox properties of the former. Weng et al. [98] found that the doping of copper to CeO_2 brought about a large amount of Cu-Ce interfaces, which were denoted as the active sites with higher oxygen availability and faster oxygen activation rate. Meng at al. [99] also reported that the interaction between Co_3O_4 and CeO_2 weakened the strength of Co—O bond and accelerated the formation of more oxygen vacancies at the interface, and a correlation between catalytic performances and interface amounts was proposed. Recently, for Co_3O_4-based catalysts, it had already been demonstrated by experiments and theoretical calculation, that doping metal cations with lower M-O bonding energies and larger ion radii was very effective to decrease the formation energy of oxygen vacancy [100].

In this work, XRD results (Fig. 2) showed that the presence of Bi_2O_3 suppressed the growth of Co_3O_4 crystal, which might be induced by the confinement effect of the strong interaction in interface layers between these two oxides. It was also proved by C-TPR (Fig. 5), O_2-TPD (Fig. 6) and $^{18}O_2$ exchange tests (Fig. 8) that the interaction between Co_3O_4 and Bi_2O_3 at the interface could weaken the metal-O bond strength and promote the activation and mobility of lattice oxygen. Even though in the absence of gaseous oxygen, this active lattice oxygen species was also involved in soot oxidation below 400 °C. In contrast, Co_3O_4 showed little ability of carbothermic reduction until 470 °C (Fig. 5). Meanwhile, the higher TOF values of Bi_xCo compared with those of Co_3O_4 and Bi_2O_3 also demonstrated that the interaction between Co_3O_4 and Bi_2O_3 promoted soot oxidation (Table 2).

Based on the previous studies [21,101,102] and the results presented in this work, soot oxidation processes over Co_3O_4 and Bi_xCo were discussed in detail as follow:

Generally, Co_3O_4 catalyzed carbon oxidation via a modified Mars and van Krevelen mechanism. Over Co_3O_4, the surface lattice oxygen at the contact point reacted with soot to produce oxygen vacancy, which would be preferentially replenished by O_2 gas instead of lattice oxygen transferring from the bulk, since the rate of oxygen diffusion from bulk to surface was slower than that of the adsorption and activation of gaseous oxygen [101,102], which was confirmed by the exchange reaction of $^{18}O_2$ dominantly following the R^1-mechanism on Co_3O_4 (Fig. 8). In other words, the reaction was localized at the three-phase boundary between soot,

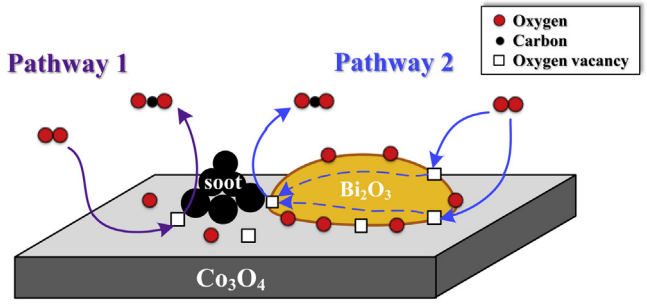

Fig. 15. Soot oxidation reaction schematic over Bi_xCo.

Co_3O_4 surface and O_2, the latter being indispensable to maintain a chemical potential gradient to push the chain of surface oxygen atoms forward to these contact points [101].

However, two situations were present on Bi_xCo. The soot contacting with Co_3O_4 surface and away from Bi-Co interface reacted with the surface oxygen on the catalyst to produce CO_2 and oxygen vacancy, and subsequently the formed oxygen vacancy was refilled by O_2 just like the case on pure Co_3O_4. While for the situation that soot contacting with Bi-Co interface or Bi_2O_3, the formed oxygen vacancy, after oxygen abstraction by soot, could be replenished by another way besides directly from gaseous oxygen. The $^{18}O_2$ exchange reaction demonstrated R^2-mechanism was dominant over $Bi_{0.2}Co$ (Fig. 8), which indicating a rapider transformation of lattice oxygen from bulk to surface. Due to the great anion conductivity and therefore the much higher migration rate of lattice oxygen in Bi_2O_3 bulk, active O^{2-} species from Bi_2O_3 could move to the contact point to replenish the produced vacancy site quickly. Along with the simultaneous reverse diffusion of vacancy (from surface to bulk), the vacancy could migrate to the other part of Bi_2O_3 surface. It undoubtedly expanded the channels for the adsorption and activation of oxygen and increased the reaction sites because the entire Bi_2O_3 surface were available for pumping oxygen from gas phase, as similar to the case of yttria-stabilized zirconia (YSZ) following the fuel-cell-type electrochemical mechanism [36]. Moreover, due to the weak metal-O bond and facile release of O_2 resulting from the interaction between Co_3O_4 and Bi_2O_3, plentiful oxygen vacancies was formed at Bi-Co interface layer even not reacting with soot, which could provide the additional channel to accelerate the transformation of active oxygen species [103–105], and further result in the higher specific rate of Bi_xCo (Table 2) than that of pure Bi_2O_3.

According to discussion above, the brief schematic of soot oxidation reaction over Bi_xCo is illustrated in Fig. 15. Pathway 1 showed the oxidation reaction at Co_3O_4/soot contact point via a redox mechanism. While, pathway 2, which was only occurred in Bi_2O_3-doped Co_3O_4, included the adsorption and activation of O_2 activation at oxygen vacancies on the surface of Bi_2O_3 and/or at the interface of Bi_2O_3 and Co_3O_4, and the migration of active oxygen species (O^{2-}) to the contact point of catalyst and soot via oxygen vacancies in Bi_2O_3 bulk, which was proved to be more effective for oxygen activation during soot oxidation reaction. Meanwhile, the high mobility of BiO_x species and the roughness of catalyst surface (Fig. 3) could produce more contact points between catalyst and soot, which could also accelerate the soot oxidation on Bi_xCo catalysts. All these jointly resulted in that Bi_xCo catalysts showed comparable or better activity than CeO_2 or doped-CeO_2 catalysts which were widely reported for soot oxidation [106–109]. Such as, the specific rate of our $Bi_{0.2}Co$ at 240 °C (5.26×10^{-8} mol s^{-1} m^{-2}) was much higher than that of the pure CeO_2 (1.40×10^{-9} mol s^{-1} m^{-2}) or Fe-doped CeO_2 ($2.25 - 3.96 \times 10^{-9}$ mol s^{-1} m^{-2}) at 280 °C [49].

The diffusion of O^{2-} ions into the lattice might be the rate-limiting step of reaction, since the formation of labelled CO_2 ($C^{18}O_2$ and $C^{18}O^{16}O$) became conspicuous only after the $C^{16}O_2$ had strongly fallen off [110].

There was an optimum in soot oxidation activity for Bi_xCo catalysts, namely $Bi_{0.2}Co$. This phenomenon was suggested to originate from the different amount of Bi-Co interfaces in Bi_xCo catalysts. There was no significant difference on TOF values among $Bi_{0.1}Co$, $Bi_{0.2}Co$ and $Bi_{0.3}Co$, therefore, the obvious different activities in TPO reactions was mostly attributed to the reactive site amounts (Table 2).

Moreover, $Bi_{0.2}Co$ catalysts also showed high stability against thermal shock (Fig. 12), H_2O (Fig. 13) and SO_2 (Table 3). The effective resistance seemed more pronounced under loose contact, which was important for practical application. The intrinsic reason of its high stability was hypothetically attributed to strong interaction between Bi_2O_3 and Co_3O_4, which was so robust to sustain the active interfaces, and this still need to be explored deeply in the future work. Anyhow, we had shown a potential catalyst exhibiting sufficient activity and stability as a substitute for the commercial platinum group metals (PGM) catalysts.

5. Conclusion

Bi-doped Co_3O_4 catalysts exhibit outstanding activity for soot oxidation by O_2. When compared with Co_3O_4, the T_{50} temperatures of $Bi_{0.2}Co$, the most active one, lower by 90 and 75 °C in tight and loose contact, respectively. It is shown that doping Co_3O_4 with Bi_2O_3 weakens the metal—O bond strength and facilitates the formation of oxygen vacancies. Moreover, the oxygen exchange mechanism changes from R^1 on pure Co_3O_4 to R^2 on $Bi_{0.2}Co$. The mobility of lattice oxygen species is accelerated and the channels of oxygen activation are extended over Bi_xCo catalysts due to the combination of the role of oxygen vacancies and the high anion conductivity of Bi_2O_3, which shows high efficiency for pumping oxygen from gas phase to soot/catalyst contact point at relatively low temperatures. In addition, the low melting point of Bi_2O_3 could also improve the contact state between catalyst and soot.

Tolerance experiments demonstrate that $Bi_{0.2}Co$ catalyst shows high thermal stability and SO_2 resistance. Meanwhile, H_2O could improve the catalytic activities, especially under loose contact condition, and the hydrothermal aging has no influence on $Bi_{0.2}Co$. All those reflect an apparent superiority for practical application.

Note

The authors declare no competing financial interest.

References

[1] M.V. Twigg, Appl. Catal. B Environ. 70 (2007) 2–15.
[2] T.J. Wallington, E.W. Kaiser, J.T. Farrell, Chem. Soc. Rev. 35 (2006) 335–347.
[3] R.M. Heck, S. Gulati, R.J. Farrauto, Chem. Eng. J. 82 (2001) 149–156.
[4] A.N. Chigapov, A.A. Dubkov, B.P. Carberry, R.W. McCabe, US 7030054 (2006).
[5] H. Muroyama, H. Asajima, S. Hano, T. Matsui, K. Eguchi, Appl. Catal. A Gen. 489 (2015) 235–240.
[6] J.K. Hochmuth, K. Wassermann, R.J. Farrauto, Car exhaust cleaning, in: K. Poeppelmeier (Ed.), Comprehensive Inorganic Chemistry II, second edition, Elsevier, Amsterdam, 2013, pp. 505–523.
[7] J. Neeft, M. Makkee, J. Moulijn, Appl. Catal. B Environ. 8 (1996) 57–78.
[8] B.A.A.L. van Setten, M. Makkee, J.A. Moulijn, Catal. Rev. 43 (2001) 489–564.
[9] E. Cauda, D. Mescia, D. Fino, G. Saracco, V. Specchia, Ind. Eng. Chem. Res. 44 (2005) 9549–9555.
[10] E. Aneggi, D. Wiater, C. de Leitenburg, J. Llorca, A. Trovarelli, ACS Catal. 4 (2014) 172–181.
[11] Y.C. Wei, J. Liu, Z. Zhao, Y.S. Chen, C.M. Xu, A.J. Duan, G.Y. Jiang, H. He, Angew. Chem. 50 (2011) 2326–2329.
[12] F.E. Tuler, E.M. Gaigneaux, E.E. Miró, V.G. Milt, D.P. Debecker, Catal. Commun. 72 (2015) 116–120.
[13] B.Y. Bai, H. Arandiyan, J.H. Li, Appl. Catal. B Environ. 142 (2013) 677–683.

[14] Q. Wang, Y. Peng, J. Fu, G.Z. Kyzas, S.M.R. Billah, S.Q. An, Appl. Catal. B Environ. 168–169 (2015) 42–50.
[15] S.A. Singh, G. Madras, Appl. Catal. A Gen. 504 (2014) 463–475.
[16] G. Salek, P. Alphonse, P. Dufour, S. Guillemet-Fritsch, C. Tenailleau, Appl. Catal. B Environ. 147 (2014) 1–7.
[17] B. de Rivas, R. López-Fonseca, C. Jiménez-González, J.I. Gutiérrez-Ortiz, J. Catal. 281 (2011) 88–97.
[18] L.H. Hu, K.Q. Sun, Q. Peng, B.Q. Xu, Y.D. Li, Nano Res. 3 (2010) 363–368.
[19] X.W. Xie, Y. Li, Z.Q. Liu, M. Haruta, W.J. Shen, Nature 458 (2009) 746–749.
[20] Y. Lou, J. Ma, X.M. Cao, L. Wang, Q.G. Dai, Z.Y. Zhao, Y.F. Cai, W.C. Zhan, Y. Guo, P. Hu, G.Z. Lu, Y.L. Guo, ACS Catal. 4 (2014) 4143–4152.
[21] P.G. Harrison, I.K. Ball, W. Daniell, P. Lukinskas, M. Cespedes, E.E. Miro, M.A. Ulla, Chem. Eng. J. 95 (2003) 47–55.
[22] J. Liu, Z. Zhao, J.Q. Wang, C.M. Xu, A.J. Duan, G.Y. Jiang, Q. Yang, Appl. Catal. B Environ. 84 (2008) 185–195.
[23] P.A. Kumar, M.D. Tanwar, N. Russo, R. Pirone, D. Fino, Catal. Today 184 (2012) 279–287.
[24] M. Dhakad, T. Mitshuhashi, S. Rayalu, P. Doggali, S. Bakardjiva, J. Subrt, D. Fino, H. Haneda, N. Labhsetwar, Catal. Today 132 (2008) 188–193.
[25] B.A.A.L. van Setten, J.M. Schouten, M. Makkee, J.A. Moulijn, Appl. Catal. B Environ. 28 (2000) 253–257.
[26] Y.F. Yu, M. Meng, F.F. Dai, Nanoscale 5 (2013) 904–909.
[27] M. Galvez, S. Ascaso, R. Moliner, M. Lazaro, Top. Catal. 56 (2013) 493–498.
[28] B. Ura, J. Trawczynski, A. Kotarba, W. Bieniasz, M.J. Illan-Gomez, A. Bueno-Lopez, F.E. Lopez-Suarez, Appl. Catal. B Environ. 101 (2011) 169–175.
[29] L.N. Sui, L.Y. Yu, Chem. Eng. J. 155 (2009) 508–513.
[30] R. Kimura, S.P. Elangovan, M. Ogura, H. Ushiyama, T. Okubo, J. Phys. Chem. C 115 (2011) 14892–14898.
[31] H. Wang, J. Liu, Z. Zhao, Y.C. Wei, C.M. Xu, Catal. Today 184 (2012) 288–300.
[32] Q. Shen, M.F. Wu, H. Wang, C. He, Z.P. Hao, W. Wei, Y.H. Sun, Catal. Sci. Technol. 5 (2015) 1941–1952.
[33] G.C. Zou, Y. Xu, S.J. Wang, M.X. Chen, W.F. Shangguan, Catal. Sci. Technol. 5 (2015) 1084–1092.
[34] E. Aneggi, C. de Leitenburg, A. Trovarelli, Catal. Today 181 (2012) 108–115.
[35] M. Sun, L. Wang, B.N. Feng, Z.G. Zhang, G.Z. Lu, Y. Guo, Catal. Today 175 (2011) 100–105.
[36] E. Obeid, L. Lizarraga, M.N. Tsampas, A. Cordier, A. Boreave, M.C. Steil, G. Blanchard, K. Pajot, P. Vernoux, J. Catal. 309 (2014) 87–96.
[37] P. Shuk, H.D. Wiemhöfer, U. Guth, W. Göpel, M. Greenblatt, Solid State Ionics 89 (1996) 179–196.
[38] M.G. Hapase, V.B. Tare, A.B. Biswas, Ind. J. Pure Appl. Phys. 5 (1967) 401.
[39] N. Imanaka, T. Masui, K. Minami, K. Koyabu, Chem. Mater. 17 (2005) 6511–6513.
[40] B. Bassou, N. Guilhaume, E.E. Iojoiu, D. Farrusseng, K. Lombaert, D. Bianchi, C. Mirodatos, Catal. Today 159 (2011) 138–143.
[41] K. Minami, T. Masui, N. Imanaka, L. Dai, B. Pacaud, J. Alloys Compd. 408–412 (2006) 1132–1135.
[42] Y. Lou, L. Wang, Y.H. Zhang, Z.Y. Zhao, Z.G. Zhang, G.Z. Lu, Y. Guo, Catal. Today 175 (2011) 610–614.
[43] T. Ishihara, T. Oishi, S. Hamamoto, Catal. Commun. 10 (2009) 1722–1724.
[44] M.A. Peralta, M.S. Zanuttini, C.A. Querini, Appl. Catal. B Environ. 110 (2011) 90–98.
[45] M.A. Peralta, V.G. Milt, L.M. Cornaglia, C.A. Querini, J. Catal. 242 (2006) 118–130.
[46] S.J. Park, H.A. Ahn, I.J. Heo, I.-S. Nam, J.H. Lee, Y.K. Youn, H.J. Kim, Top. Catal. 53 (2010) 57–63.
[47] H.N. Sharma, L. Pahalagedara, A. Joshi, S.L. Suib, A.B. Mhadeshwar, Energy Fuels 26 (2012) 5613–5625.
[48] L. Pahalagedara, H. Sharma, C.-H. Kuo, S. Dharmarathna, A. Joshi, S.L. Suib, A.B. Mhadeshwar, Energy Fuels 26 (2012) 6757–6764.
[49] Z.L. Zhang, D. Han, S.J. Wei, Y.X. Zhang, J. Catal. 276 (2010) 16–23.
[50] J.F. Xu, J. Liu, Z. Zhao, C.M. Xu, J.X. Zheng, A.J. Duan, G.Y. Jiang, J. Catal. 282 (2011) 1–12.
[51] C.J. Jia, M. Schwickardi, C. Weidenthaler, W. Schmidt, S. Korhonen, B.M. Weckhuysen, F. Schuth, J. Am. Chem. Soc. 133 (2011) 11279–11288.
[52] G.Q. Zhu, J. Lian, M. Hojamberdiev, W.X. Que, J. Clust. Sci. 24 (2013) 829–841.
[53] J. In, I. Yoon, K. Seo, J. Park, J. Choo, Y. Lee, B. Kim, Chem. Eur. J. 17 (2011) 1304–1309.
[54] B.Y. Bai, J.H. Li, ACS Catal. 4 (2014) 2753–2762.
[55] N. Russo, S. Furfori, D. Fino, G. Saracco, V. Specchia, Appl. Catal. B Environ. 83 (2008) 85–95.
[56] N. Merino, B. Barbero, P. Grange, L. Cadus, J. Catal. 231 (2005) 232–244.
[57] Z.L. Zhang, Y.X. Zhang, Q.Y. Su, Z.P. Wang, Q. Li, X.Y. Gao, Environ. Sci. Technol. 44 (2010) 8254–8258.
[58] V. Botu, R. Ramprasad, A.B. Mhadeshwar, Surf. Sci. 619 (2014) 49–58.
[59] D.Y. Yoon, E. Lim, Y.J. Kim, J.H. Kim, T. Ryu, S. Lee, B.K. Cho, I.-S. Nam, J.W. Choung, S. Yoo, J. Catal. 319 (2014) 182–193.
[60] B.M. Reddy, L. Katta, G. Thrimurthulu, Chem. Mater. 22 (2010) 467–475.
[61] C. Doornkamp, M. Clement, V. Ponec, J. Catal. 182 (1999) 390–399.
[62] E.M. Sadovskaya, Y.A. Ivanova, L.G. Pinaeva, G. Grasso, T.G. Kuznetsova, A. van Veen, V.A. Sadykov, C. Mirodatos, J. Phys. Chem. A 111 (2007) 4498–4505.
[63] C.C. Kan, H.H. Kan, F.M. Van Assche, E.N. Armstrong, E.D. Wachsman, J. Electrochem. Soc. 155 (2008) B985.
[64] S. Royer, D. Duprez, S. Kaliaguine, J. Catal. 234 (2005) 364–375.
[65] S. Adler, X. Chen, J. Wilson, J. Catal. 245 (2007) 91–109.
[66] H. He, H.X. Dai, C.T. Au, Catal. Today 90 (2004) 245–254.
[67] Y. Gao, A. Duan, S. Liu, X. Wu, W. Liu, M. Li, S. Chen, X. Wang, D. Weng, Appl. Catal. B Environ. 203 (2017) 116–126.
[68] S. Hernández, G.A. Blengini, N. Russo, D. Fino, Ind. Eng. Chem. Res. 51 (2012) 7584–7589.
[69] K. Harada, T. Oishi, S. Hamamoto, T. Ishihara, J. Phys. Chem. C 118 (2014) 559–568.
[70] R.Y. Zhong, K.Q. Sun, Y.C. Hong, B.Q. Xu, ACS Catal. 4 (2014) 3982–3993.
[71] S. Mosconi, I.D. Lick, A. Carrascuii, M.I. Ponzi, E.N. Ponzi, Catal. Commun. 8 (2007) 1755–1758.
[72] A. Bueno-López, A. García-García, Energy Fuels 19 (2005) 94–100.
[73] M.A. Peralta, M.A. Ulla, C.A. Querini, Catal. Today 133 (2008) 461–466.
[74] J. Oi-Uchisawa, A. Obuchi, A. Ogata, R. Enomoto, S. Kushiyama, Appl. Catal. B Environ. 21 (1999) 9–17.
[75] M.L. Fu, X.H. Yue, D.Q. Ye, J.H. Ouyang, B.C. Huang, J.H. Wu, H. Liang, Catal. Today 153 (2010) 125–132.
[76] H.N. Sharma, V. Sharma, A.B. Mhadeshwar, R. Ramprasad, J. Phys. Chem. Lett. 6 (2015) 1140–1148.
[77] Z.Q. Zou, M. Meng, N. Tsubaki, J.J. He, G. Wang, X.G. Li, X.Y. Zhou, J. Hazard. Mater. 170 (2009) 118–126.
[78] T. Jin, T. Yamaguchi, K. Tanabe, J. Phys. Chem. 90 (1986) 4794–4796.
[79] T. Saison, N. Chemin, C. Chanéac, O. Durupthy, V. Ruaux, L. Mariey, F. Maugé, P. Beaunier, J.P. Jolivet, J. Phys. Chem. C 115 (2011) 5657–5666.
[80] S. Liu, X.D. Wu, D. Weng, M. Li, R. Ran, ACS Catal. 5 (2015) 909–919.
[81] J.P.A. Neeft, O.P. van Pruissen, M. Makkee, J.A. Moulijn, Appl. Catal. B Environ. 12 (1997) 21–31.
[82] E.E. Iojoiu, B. Bassou, N. Guilhaume, D. Farrusseng, A. Desmartin-Chomel, K. Lombaert, D. Bianchi, C. Mirodatos, Catal. Today 137 (2008) 103–109.
[83] M.A. Peralta, M.S. Zanuttini, M.A. Ulla, C.A. Querini, Appl. Catal. A Gen. 399 (2011) 161–171.
[84] R. Matarrese, L. Castoldi, N. Artioli, E. Finocchio, G. Busca, L. Lietti, Appl. Catal. B Environ. 144 (2014) 783–791.
[85] V. Serra, G. Saracco, C. Badini, V. Specchia, Appl. Catal. B Environ. 11 (1997) 329–346.
[86] N.W. Piekiel, L. Zhou, K.T. Sullivan, S. Chowdhury, G.C. Egan, M.R. Zachariah, Combust. Sci. Technol. 186 (2014) 1209–1224.
[87] N.W. Piekiel, G.C. Egan, K.T. Sullivan, M.R. Zachariah, J. Phys. Chem. C 116 (2012) 24496–24502.
[88] Bismuth oxide (Bi_2O_3) heat capacity, density, melting point, in: O. Madelung, U. Rössler, M. Schulz (Eds.), Non-Tetrahedrally Bonded Elements and Binary Compounds I, Springer, Berlin, 1998, pp. 1–2.
[89] E.W. McFarland, H. Metiu, Chem. Rev. 113 (2013) 4391–4427.
[90] Z. Zhou, S. Kooi, M. Flytzani-Stephanopoulos, H. Saltsburg, Adv. Funct. Mater. 18 (2008) 2801–2807.
[91] M. Haneda, A. Towata, Catal. Today 242 (2014) 351–356.
[92] M. Konsolakis, Appl. Catal. B Environ. 198 (2016) 49–66.
[93] D. Mukherjee, B.G. Rao, B.M. Reddy, Appl. Catal. B Environ. 197 (2016) 105–115.
[94] G.N. Li, L. Li, Y. Yuan, J.J. Shi, Y.Y. Yuan, Y.S. Li, W.R. Zhao, J.L. Shi, Appl. Catal. B Environ. 158 (2014) 341–347.
[95] K. Yamazaki, T. Kayama, F. Dong, H. Shinjoh, J. Catal. 282 (2011) 289–298.
[96] T. Kayama, K. Yamazaki, H. Shinjoh, J. Am. Chem. Soc. 132 (2010) 13154–13155.
[97] F.E. López-Suárez, A. Bueno-López, M.J. Illán-Gómez, A. Adamski, B. Ura, J. Trawczynski, Environ. Sci. Technol. 42 (2008) 7670–7675.
[98] D. Weng, J. Li, X.D. Wu, F. Lin, Catal. Commun. 9 (2008) 1898–1901.
[99] J.Y. Luo, M. Meng, X. Li, X.G. Li, Y.Q. Zha, T.D. Hu, Y.N. Xie, J. Zhang, J. Catal. 254 (2008) 310–324.
[100] Y. Lou, X.M. Cao, J.G. Lan, L. Wang, Q.G. Dai, Y. Guo, J. Ma, Z.Y. Zhao, Y.L. Guo, P. Hu, G.Z. Lu, Chem. Commun. 50 (2014) 6835–6838.
[101] G. Mul, F. Kapteijn, C. Doornkamp, J.A. Moulijn, J. Catal. 179 (1998) 258–266.
[102] G. Mul, J.P.A. Neeft, F. Kapteijn, J.A. Moulijn, Carbon 36 (1998) 1269–1276.
[103] C.H. Zhang, C. Wang, W.C. Zhan, Y.L. Guo, Y. Guo, G.Z. Lu, A. Baylet, A. Giroir-Fendler, Appl. Catal. B Environ. 129 (2013) 509–516.
[104] C. Descorme, Y. Madier, D. Duprez, J. Catal. 196 (2000) 167–173.
[105] S. Wagloehner, S. Kureti, Appl. Catal. B Environ. 125 (2012) 158–165.
[106] M. Machida, Y. Murata, K. Kishikawa, D.J. Zhang, K. Ikeue, Chem. Mater. 20 (2008) 4489–4494.
[107] V. Di Sarli, G. Landi, L. Lisi, A. Saliva, A. Di Benedetto, Appl. Catal. B Environ. 197 (2016) 116–124.
[108] E. Aneggi, N.J. Divins, C. de Leitenburg, J. Llorca, A. Trovarelli, J. Catal. 312 (2014) 191–194.
[109] A. Bueno-López, Appl. Catal. B Environ. 146 (2014) 1–11.
[110] N. Guilhaume, B. Bassou, G. Bergeret, D. Bianchi, F. Bosselet, A. Desmartin-Chomel, B. Jouguet, C. Mirodatos, Appl. Catal. B Environ. 119 (2012) 287–296.